Topographic Effects on Bidirectional and Hemispherical Reflectances Calculated with a Geometric-Optical Canopy Model

Crystal Barker Schaaf, *Member, IEEE*, Xiaowen Li, and Alan H. Strahler, *Member, IEEE*

***Abstract*—The effects of topography on both the Bidirectional Reflectance Distribution Function (BRDF) and the hemispherical reflectance (surface albedo) of a forested scene are investigated with the Li–Strahler geometric-optical model. The Li–Strahler geometric-optical model treats a vegetation canopy as an assemblage of partially illuminated tree crowns of spheroidal shape, and through geometric optics and Boolean set theory, models the proportion of sunlit or shadowed canopy and background as functions of view angle, illumination angle, and crown geometry. The model has been modified to accommodate a sloping surface in its computation of bidirectional and hemispherical reflectance. When the BRDF of a flat vegetated surface is compared to the BRDF of a sloping surface that is similarly vegetated, the interaction of the illumination angle and the slope distort the shape of the BRDF. A hemispherical integration of this distorted BRDF provides an albedo for the sloping surface.**

***Index Terms*—Hemispherical reflectance, surface albedo, bidirectional reflectance distribution function, topography, canopy reflectance modeling**

I. Introduction

The anisotropy of vegetated surfaces has been well documented though a number of measurement studies [1]–[3] and explored through a variety of radiative transfer studies [4]–[10], radiosity and ray tracing simulations [11]–[14] and geometric-optical modeling [15]–[19]. These works assume that the terrain and the overlying canopy are flat. However, a space based sensor collects radiation from a variety of sloping surfaces and, depending on the resolution of the field of view, the signal can be primarily influenced by terrain shadowing, view factor effects, and/or the aspect and steepness of individual slopes.

In this study, the influence of individual vegetated slopes will be investigated using the Li–Strahler geometric-optical model [15]–[17]. The Li–Strahler geometric-optical model treats a scene as an assemblage of spheroidal tree crowns. Geometric-optics and Boolean set theory are used to determine the areal proportions of shadowed and sunlit canopy and shadowed and sunlit background associated with a particular view angle under given illumination conditions. These areal proportions are weighted by independently-determined characteristic spectral signatures for each of the shadowed or sunlit components and are used to determine the spectral bidirectional reflectance factor of the canopy. The model captures the "hotspot" effect—the peak in directional reflectance in the backscatter direction that occurs when the viewer of a forested canopy is in the same angular position as the sun and all visible portions of the scene are illuminated and unshadowed. Moving away from the hotspot direction, more and more shadows are revealed and the directional reflectance values decrease as the azimuthal position of the viewer changes with respect to the sun. At very high solar or view zenith angles, the model incorporates the mutual shadowing effect that can cause the directional reflectance values to again increase. In a hemispherical representation of the BRDF, this effect produces a "bowl shape" in the forward scatter region. Mutual shadowing, and its resultant brightening of the scene, occurs at angles where only the tree tops are illuminated and any shadows are lost in the lower part of the canopy and obscured by other tree crowns.

This paper documents how the Li–Strahler mutual shadowing model can be extended to compute the bidirectional and hemispherical reflectance of vegetation on complex terrain. In essence, the model transforms the geometric relationships among the illumination angle, the view angle, and all of the tree shape characteristics into the coordinate system of the slope, so that the problem reduces to that of mutual shadowing on a flat surface. The resultant BRDF is then transformed back into true space, where a hemispherical integration takes place to produce an albedo. The computations assume that the model domain (simulating a sensor field of view or pixel) is the same or smaller than the slope. With the model accommodating topography, it is possible to compute the direct beam albedo for a variety of slopes and aspects. Realistic tree shape parameters and component signatures for a conifer canopy, based on extensive fieldwork in the Sierra Nevada of California [20], are used in these simulations.

II. Model Enhancements

A. Topography Transformations

To apply the Li–Strahler geometric-optical model (see Appendix) to sloping terrain, several transformations in coor-

Manuscript received January 10, 1994. This work was supported by NASA awards NAGW-1474 and NAS5-31369.

C. Barker Schaaf is with the Geophysics Directorate, Phillips Laboratory, Hanscom AFB, MA 01731 USA.

X. Lin is with the Institute of Remote Sensing Application, Chinese Academy of Science, Beijing. He is currently with the Center for Remote Sensing, Boston University, Boston, MA 02215 USA.

A. H. Strahler is with the Department of Geography and Center for Remote Sensing, Boston University, Boston, MA 02215 USA.

IEEE Log Number 9405530.

dinate space are required. Given a solar zenith angle θ_i, a view zenith angle θ_v, a solar azimuth ϕ_i, a slope elevation θ_s, and a slope aspect ϕ_s (Fig. 1(a)), the first transformation replaces θ_i, θ_v, and θ_s with θ_i', θ_v', and θ_s', where the tree crown elongated spheroids are replaced with spheres which cast the same shadow area (Fig. 1(b)). The θ_s' is given as

$$\theta_s' = \frac{\pi}{2} - \tan^{-1}\left(\frac{b}{R}\tan\left(\frac{\pi}{2} - \theta_s\right)\right). \tag{1}$$

Once all the tree crowns are represented by spheres (and the trunks ignored), it is a simple matter to perform a second transformation and convert the entire scene to slope coordinates and then compute the BRDF in that coordinate system (Fig. 1(c)). In the slope coordinate system, the Y axis remains the same and the scene is rotated about it. The slope normal becomes the Z' axis, and the X' axis runs along the surface of the slope. The slope ϕ_s is set to zero. The solar angles are then recalculated in relation to these slope coordinates:

$$\phi_i' = \phi_i - \phi_s \tag{2}$$

and

$$x' = \cos\phi_i' \sin\theta_i' \cos\theta_s' - \cos\theta_i' \sin\theta_s' \tag{3}$$

$$y' = \sin\phi_i' \sin\theta_i' \tag{4}$$

$$z' = \cos\phi_i' \sin\theta_i' \sin\theta_s' + \cos\theta_i' \cos\theta_s' \tag{5}$$

resulting in transformed solar angles of

$$\theta_i'' = \cos^{-1} z' \tag{6}$$

$$\phi_i'' = \tan^{-1}\frac{y'}{x'}. \tag{7}$$

Once all of the illumination angles are transformed, the scene can be treated as a flat surface and the BRDF can be calculated as usual with the principal plane located where $\theta_v'' = \phi_i''$ or $\theta_v'' = \phi_i'' + \pi$. This will result in a reflectance for each view zenith θ_v'' and view azimuth ϕ_v''. These reflectances can then be associated back to coordinates in true space by transforming them with

$$x' = \sin\theta_v'' \cos\phi_v'' \tag{8}$$

$$y' = \sin\theta_v'' \sin\phi_v'' \tag{9}$$

$$z' = \cos\theta_v'' \tag{10}$$

and

$$\phi_v' = \tan^{-1}\left(\frac{y'\sin\theta_s' + \cot\theta_s' + \cos\theta_s' y'}{z + \cot\theta_s' x'}\right) \tag{11}$$

$$\theta_v' = \sin^{-1}\left(\frac{y'}{\sin\phi_v'}\right). \tag{12}$$

Finally, by adding the slope aspect, the angles are relative to true compass directions and, by transforming the crown spheres back into elongated spheroids, each reflectance is associated with a true view zenith (θ_v) and true view azimuth (ϕ_v). At this point it is possible to perform a hemispherical integration and produce a direct beam albedo for the forested slope.

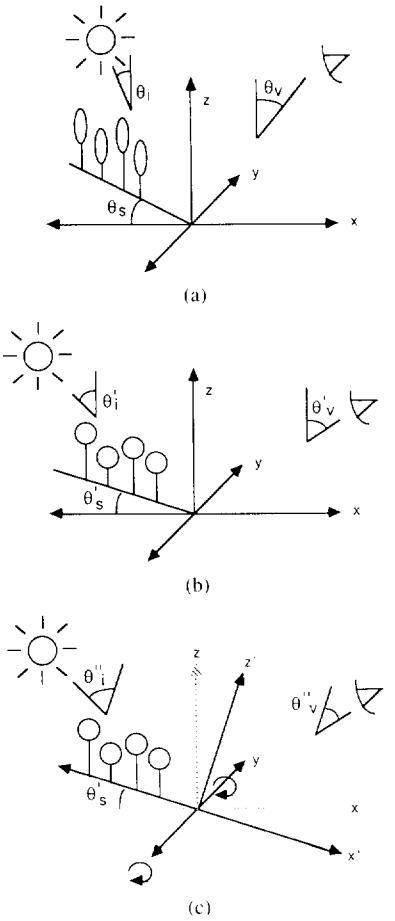

Fig. 1. Schematic depicting the coordinate system transformations required within the geometric-optical model to accommodate a sloping surface. The illumination, view, and slope angles in the original coordinate system (a) are transformed to prime angles (b). This transformation allows crowns to be treated as spheres and cast the same shadow areas as they did as elongated spheroids. The angles are further transformed to double prime angles when the scene is considered in terms of the slope coordinate system (c).

III. Simulations

A. Inputs

To explore the effects of the new topographic transformations on canopy BRDF's and albedos, realistic tree shape parameters and component signatures for a conifer canopy (based on extensive fieldwork in the Sierra Neavada of California [20]) were used to initialize the geometric-optical model (the actual values used are given in Table I). A density of 162 trees per hectare (or 50% coverage) was simulated. Southeastly solar angles, appropriate for a July morning in the Sierra Nevada ($\theta_i = 31.21°$ and $\phi_i = 338.6°$), were used. A flat surface was modeled, as well as two slope elevations (a slope of 16° and a steep slope of 30°) with aspects facing in the four compass directions.

B. Results

The BRDF describes the intrinsic character of the canopy surface under any given solar illumination. As revealed in the spectral BRDF's of flat surfaces (Figs. 2(a)–(b)), the hotspot peak occurs when the viewing position approaches

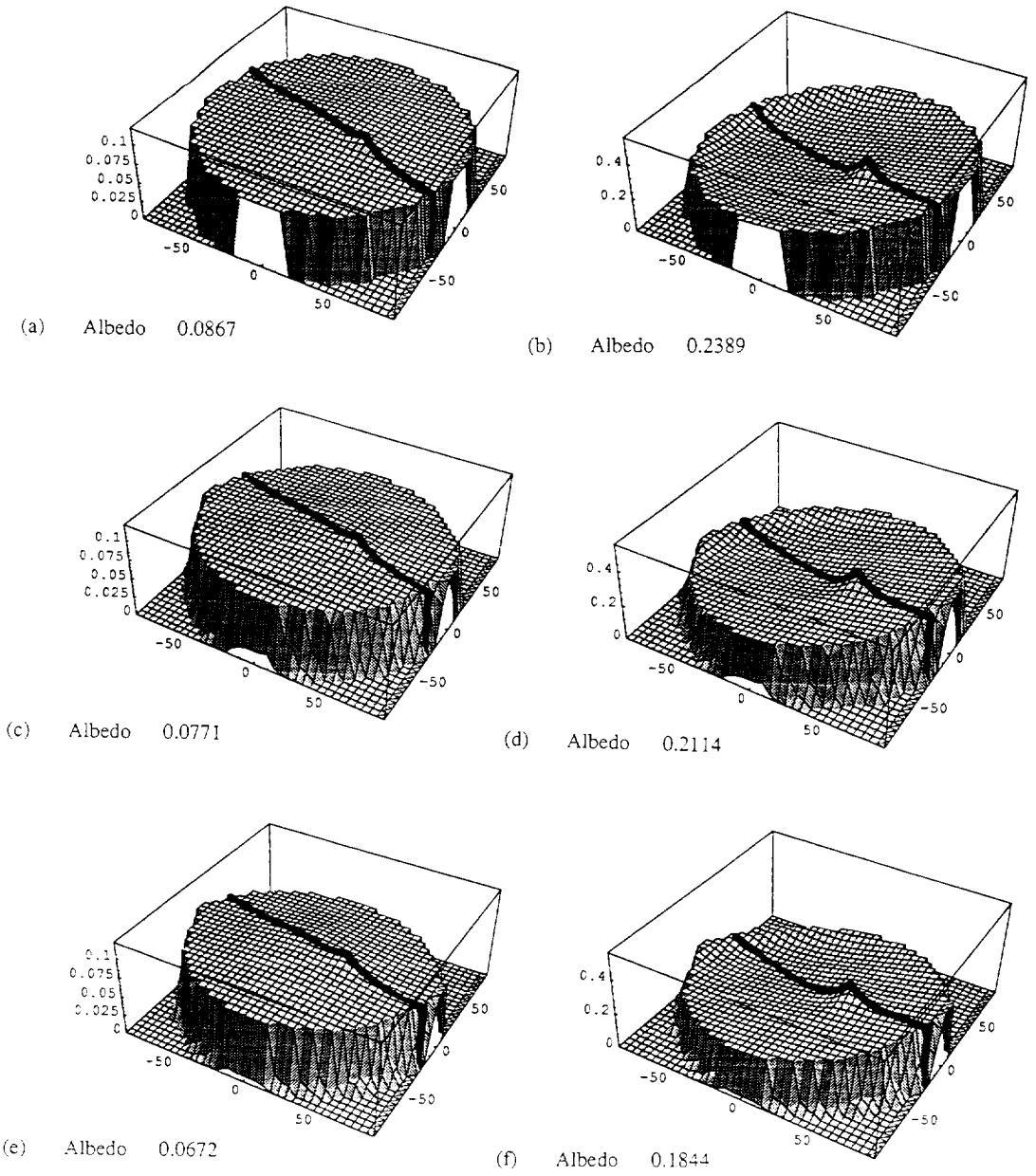

Fig. 2. Red and near-infrared BRDF simulations of a conifer canopy on flat terrain (a), (b), on a 16° slope (c), (d), and on a 30° slope (e), (f). The sloping surfaces are facing south. Each three-dimensional BRDF is displayed in rectangular coordinate system where each view angle in the hemisphere is taken as a prior of polar coordinates and transformed onto the x-y plane as a vector of unit length. The corresponding reflectances are then plotted along the z axis.

TABLE I
CANOPY PARAMETERS

Signature	red	NIR
C	0.074	0.36
G	0.15	0.33
Z	0.084	0.099
$h = 22$ m ± 7 m		
$b = 9.8$ m		
$r = 3.7$ m		

the illumination angle. Its shape is governed by the brightness contrast between tree crown and background and by the shape and density of the crowns and the rapidity with which the shadows they cast are revealed when the viewing and illumination geometry diverge. Opposite the hotspot (in the forward scattering direction), increasingly large areas of shadow (with lower reflectances) are viewed. The upturned bowl-shape is produced when the proportion of viewed shadows is reduced by the obscuring of these shadows by nearby crowns (i.e., the scene brightens at the large view angles, as only unshadowed crown tops are viewed). This mutual shadowing occurs at either high illumination or high viewing zenith angle (or both) and more so for those crown shapes that present a larger cross section at higher zenith angles (tall thinner crown shapes). Mutual shadowing enhances reflectance more in the near-infrared, where the unshadowed crowns have brighter signatures.

Once the canopy is draped over a slope, the shape of the BRDF changes (Figs. 2(c)–(f)). Figs. 2(c) (red wavelength) and 2(d) (near-infrared) depict the 16° southerly facing slope while Figs. 2(e) and 2(f) represent the steeper 30° slope. The

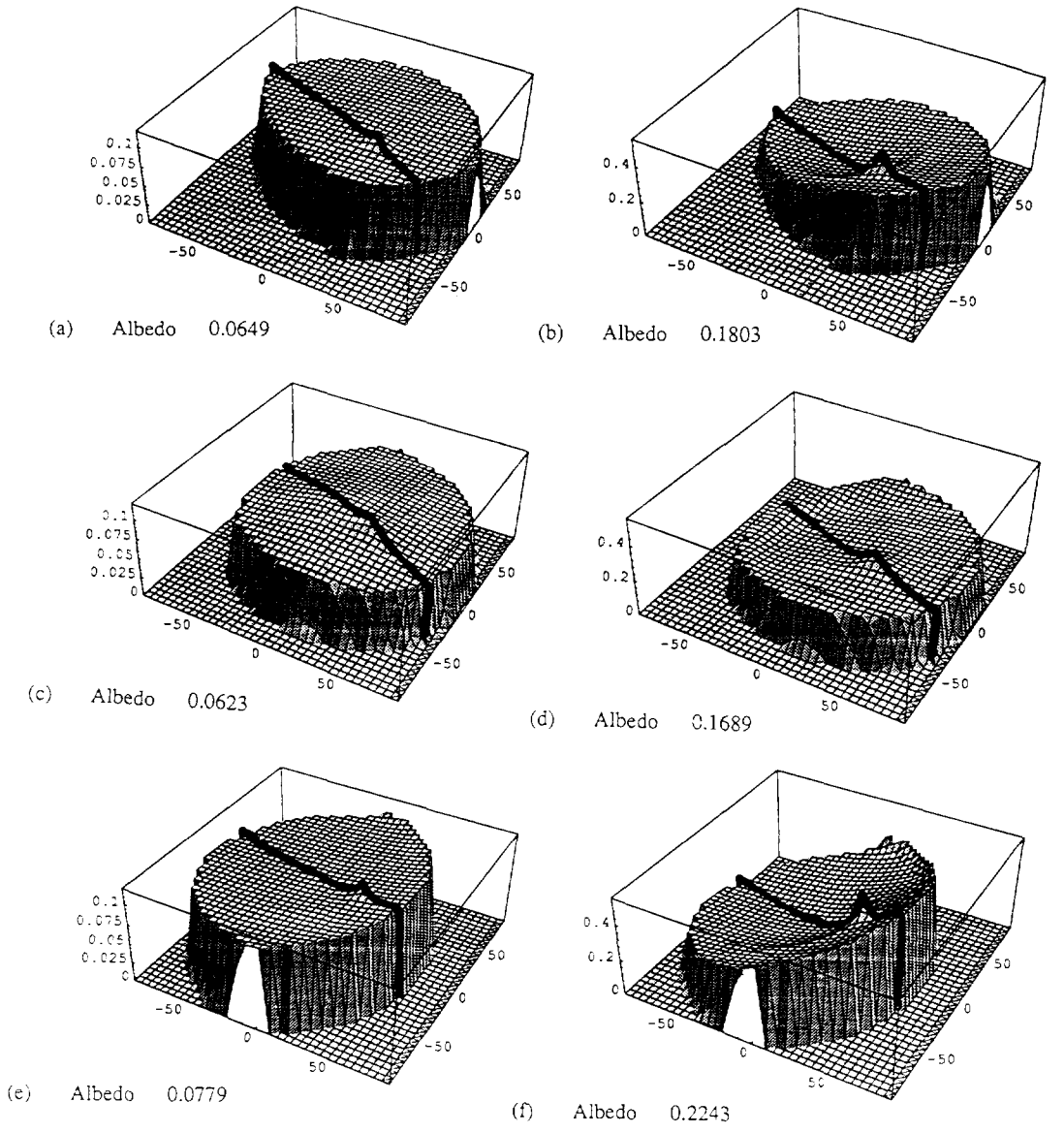

Fig. 3. Red and near-infrared BRDF simulations of a conifer canopy on a 30° slope facing north (a), (b), east (c), (d), and west (e), (f).

hotspot still occurs at the same location, regardless of slope. The forward scatter radiation, however, is forced into a skewed direction governed by the elevation and aspect of the slope. Therefore the principal plane may now veer along from the hotspot into the shadowing region. The crown shadowing is governed by the difference between the slope normal and the solar angle rather than the solar angle itself. The view angles engulfed by the slope mass are of course not represented. Similarly, the reflectances from view angles that would be below the horizontal are set to zero. As stated earlier, the model assumes the pixels are smaller or the same size as the slope, and no additional view factor radiation from nearby terrain is incorporated.

Figs. 3(a)–(f) reveal the spectral BRDF distortion that occurs as the aspect on the steep slopes is swiveled through the remaining compass directions. In all of these simulations, the sun is high enough in the sky that no terrain shadowing is occurring and, regardless of the slope aspect, the canopy is directly illuminated.

The spectral hemispherical reflectances (or direct beam surface albedos) derived with each BRDF are also noted on Figs. 2(a)–(f) and 3(a)–(f). The flat terrain hemispherical reflectance is the largest albedo value associated with this canopy. This occurs because the flat case is the only one where a nonzero reflectance value is associated with each and every possible view angle in the integrating sphere. The albedo is a rather consistent value, affected only slightly by the gentler slopes (only a 12% variation in albedo on 16° slopes with differing aspects). On the steeper slopes (30°), however, the albedo is more sensitive to aspect. Note that the slopes that face away from the sun and receive less direct solar radiation, are, however, associated with larger albedos than the slopes that face the sun. This occurs because of changes in the shadowing patterns and an increase in mutual shadowing. The sun, when it is regarded in slope coordinates, achieves very large solar zenith angles on slopes facing away from the sun. Mutual shadowing usually increases (enough so that the overall

hemispherical reflectance also increases) as the solar zenith angle increases.

IV. Conclusion

A variety of schemes exist to remove the effect of topography from remotely sensed images [21]–[26] and the importance of using a non-Lambertian surface model to correct satellite imagery has been stressed. This study investigates the impact sloping surfaces have on the intrinsic reflective character of these non-Lambertian surfaces. In the case of forest canopies, the sloping surface significantly changes the pattern of sunlight and shadows being cast by and on individual trees and therefore changes both the bidirectional reflectance distribution function and the hemispherical reflectance associated with that canopy. The Li–Strahler geometric-optical model has been extended to incorporate sloping surfaces and is used here to explore these changes.

In simulations of conifer canopies on gentle to moderate slopes (16°), the shape of the BRDF is found to change, although the hemispherical reflectance remains rather consistent. On steeper slopes (30°), the shape of the BRDF becomes quite distorted and there is a distinct variation in the albedo values. Overall, the largest albedo values are associated with flat terrain. When comparing slopes with the same elevation but different aspects, the slopes facing away from the sun exhibit increased mutual shadowing and therefore display larger albedos than do the sunward facing slopes. These simulations indicate that, although an assumption of flat terrain may result in somewhat of an overestimation of surface albedo, such as assumption is not unreasonable since the impact of gentle to moderate slopes on surface albedo is small. This would suggest that the albedo of a forest canopy which exhibits consistent type and structure characteristics over a large region may also exhibit a fairly uniform albedo over this same area even if the underlying terrain is undulating. In regions of more rugged terrain, however, forest albedos will vary significantly as the values will be affected not only by changes in the shadowing geometries of the canopy, but also by terrain shadowing effects and the receipt of scattered radiation from adjoining slopes. Neither of the latter two macro-level three-dimensional effects is handled by the Li–Strahler geometric-optical model.

The distortion in the shape of the BRDF, as revealed by these simulations of steep forested slopes, identifies a possible difficulty in attempting to invert remotely sensed directional data to obtain surface shape and roughness characteristics. In areas of significant slope, the BRDF will no longer be symmetrical about the principal plane. If only a few directional measurements exist across such a region, it will be more difficult to reliably reconstruct the BRDF than it would have been from a similarly vegetated flat region.

Appendix

A. Geometric-Optical Model

As in [16], [17], the BRDF of a pixel is modeled as the limit of its directional reflectance factor $R(i, v)$:

$$R(i, v) = \frac{\int\int_A R(s)\langle i, s\rangle\langle v, s\rangle I_i(s) I_v(s)\, ds}{A \cos\theta_i \cos\theta_v} \tag{1A}$$

where ds is a small Lambertian surface element within area A of a pixel; $R(s)$ is the reflectance of ds; i, v, and s represent the directions of illumination, viewing, and the normal to a surface element, respectively; $\langle .. \rangle$ is the cosine of the phase angle between two directions; θ is the zenith angle of a direction; $I_i(s)$ and $I_v(s)$ are indicator functions, equal to one if ds is illuminated (I_i) or viewed (I_v), zero otherwise. Here the double integral shows that ds is integrated over the pixel.

If we assume the scene area A is apportioned into three types of surface, sunlit crown (which has the average uniform reflectance C), sunlit background (reflectance G), and shadows (reflectance Z), we can may then write (1A) in simplified form as

$$R(i, v) = K_g G + K_c C + K_z Z \tag{2A}$$

where K_g is the proportion of background both illuminated and viewed, K_c is the proportion of crown area both illuminated and viewed, and K_z is the proportion of the scene in shadow (note that here, for simplicity, the shadows, whether cast on canopy or on background, are treated the same). The first term describes how the sunlit background proportion reaches a maximum when viewing and illumination positions in the hemisphere coincide. The second term describes how the sunlit crown surface (assumed to be made up of Lambertian facets) also reaches a maximum at the hotspot, and how those facets on the tops of the crowns become dominant at large viewing and illumination zenith angles (mutual shadowing). Finally, the third term captures the contribution to the overall reflectance of the scene from the shadowed regions (since shadows are not entirely black and nonreflective).

The trees modeled in a scene or pixel are assumed to have crowns shaped as elongated spheroids, with a vertical radius equal to b, a horizontal radius equal to R, and height to the center of the spheroid h. The elongated spheroidal shapes are transformed to sphere with the relationship

$$\theta' = \tan^{-1}\left(\frac{b}{R}\tan\theta\right). \tag{3A}$$

This simply replaces θ with the angle θ', where θ' generates the same shadow area for a sphere that θ does for an elongated spheroid. The centers of the spheroids are randomly distributed in depth from h_1 to h_2 over the scene.

The K_g proportion can be expressed easily using the Boolean model [18]:

$$K_g = e^{-\lambda\pi R^2[\sec\theta_i' + \sec\theta_v' - O(\theta_i, \theta_v, \phi)]} \tag{4A}$$

where $O(\theta_i, \theta_v, \phi)$ describes the overlap between the illumination shadow and the viewing shadow (the background obscured from view by the crown itself) of individual crowns as they are projected onto the background. Here, λ is the crown count density, and ϕ is the relative azimuth angle between viewing and illumination positions.

This overlap function describes the intersected area between the two elliptical shadows. On the principal plane (PP), where $\phi = 0$ or π, the axes of the elliptical illumination and viewing shadows will be aligned in the same direction (at the hotspot, the viewing shadow will be superimposed over

the illumination shadow). The exact solution for the overlap function on the principal plane can be determined and is given as

$$O(\theta_i', \theta_v', PP) = (t - \sin t \cos t)(\sec\theta_i' + \sec\theta_v')/\pi \quad (5A)$$

where t is given as

$$\cos t = \frac{h|\tan\theta_i' - \tan\theta_v' \cos\phi|}{b(\sec\theta_i' + \sec\theta_v')}. \quad (6A)$$

On the principal cone (PC), where the view azimuth changes but the view zenith is equal to the solar zenith angle ($\theta_v' = \theta_i'$), an exact solution can also be obtained with

$$O(\theta_i', PC, \phi) = 2(t - \sin t \cos t)\sec\theta_i'/\pi \quad (7A)$$

where, in this case however, t is given as

$$\cos t = \frac{h}{b}\sin\theta_i' \sin\Phi \quad (8A)$$

and Φ is defined as

$$\tan\Phi = \tan\frac{\phi}{2}\sec\theta_i'. \quad (9A)$$

At the hotspot, where the principal plane and the principal cone intersect, (6A) and (8A) agree, yielding $t = \frac{\pi}{2}$.

In previous work [17], the overlap area along both the principal plane and the principal cone has been approximated by the area of an ellipse with one axis equal to the overlap length and the other equal to the crown width:

$$\hat{O}(\theta_i', \theta_v', PP) = \frac{1}{2}\left[\sec\theta_i' + \sec\theta_v' - \frac{h}{b}|\tan\theta_i' - \tan\theta_v'\cos\phi|\right]. \quad (10A)$$

This overlap approximation, however, overestimates the overlap area for view angles different from the principal plane or principal cone. Therefore a more accurate approximation for the off-principal-plane and off-principal-cone angles has been derived. The new approximation continues to produce values that agree with those on the principal plane and principal cone, yet, by making use of an area correction factor s_a, is conceptually simple. Assuming once more that the overlap ellipse has one axis equal to crown width, and the other axis equal to the shadow overlap length L:

$$L = R\left[\sec\theta_i' + \sec\theta_v' - \frac{h}{b}|\tan\theta_i' - \tan\theta_v'\cos\phi|\right]. \quad (11A)$$

the area scaling factor can be defined as the ratio of the exact principal plane overlap (5A) to the approximate solution (10A) or

$$S_\phi = \frac{O(\theta_i', \theta_v', PP)}{L/2R} \quad (12A)$$

where $\phi = 0$ or π. The area correction factor is the weighted sum of these two options and given as

$$S_a = S_0\left(1 - \frac{\phi}{\pi}\right) + S_\pi\frac{\phi}{\pi}. \quad (13A)$$

This is true as long as $S_\pi > 0$; otherwise $S_a = S_0$.

In computing appropriate overlap areas of off-principal-plane or off-principal-cone angles, the distance from the trunk base to the center of the overlap area needs to be determined to serve as a radius of rotation. Along the principal plane, the center of the overlap ellipse is given as

$$X_{\text{center}} = \frac{1}{2}\left[\frac{h}{b}(\tan\theta_i' + \tan\theta_v') + I(\sec\theta_i' - \sec\theta_v')\right] \quad (14A)$$

(with $I = -1$ if $\theta_i' > \theta_v'$ or $I = +1$ otherwise). This overlap center location is corrected so that the radius is zero at nadir and given as

$$\rho = \left|X_{\text{center}} - \left(1 + \frac{h}{b}(\tan\theta_i' - \sec\theta_i')\right) \times (\sin\theta_i' - \sin\theta_v')/2\sin\theta_i'\right|. \quad (15A)$$

The area correction factor and the center of the overlap ellipse can then be used to produce the new off-principal-plane overlap approximation (which is used as ϕ diverges from the principal plane):

$$O(\theta_i', \theta_v', \phi) = S_a(t - \sin t\cos t)L/\pi R \quad (16A)$$

where t is now calculated as

$$\cos t = 2\rho\sin\Phi/L \quad (17A)$$

and Φ, in this case, is given as

$$\tan\Phi = \tan\frac{\phi}{2}\left(\frac{L}{2R}\right). \quad (18A)$$

With the sunlit background proportion (K_g) defined, it is now necessary to determine the sunlit crown term (K_c). The K_c term must accommodate both hotspot effects and mutual shadowing effects. The proportion of the total area not already apportioned to sunlit background that can still be illuminated is given as

$$f = \frac{K_c}{1 - K_g}. \quad (19A)$$

The f ratio can be described in terms of the single crown proportion as

$$F = \frac{\Gamma_c}{\Gamma}. \quad (20A)$$

Here, a spheroidal crown will have a projected area in the view direction of $\Gamma_c = \pi R^2\sec\theta_v'$ but only $\frac{1}{2}(1 + \cos\theta_i'\cos\theta_v' + \sin\theta_i'\sin\theta_v'\cos\phi)$ of that area will be sunlit. This results in an area of sunlit crown projected in the view direction of

$$\Gamma_c = \pi R^2\frac{1}{2}(1 + \cos\theta_i'\cos\theta_v' + \sin\theta_i'\sin\theta_v'\cos\phi)\sec\theta_v'. \quad (21A)$$

The total area of viewed crown plus illumination shadow as projected onto the background will be

$$\Gamma = \pi R^2[\sec\theta_i' + \sec\theta_v' - O(\theta_i', \theta_v', \phi)]. \quad (22A)$$

If there is only one crown in the pixel, then $f = F$. In the multiple crown case, however:

$$f = \beta F\frac{(1 - \Gamma_c P_c M_c/\Gamma_c)}{1 - M} + (1 - \beta)F. \quad (23A)$$

This holds while $\theta_v' > \theta_i'$, otherwise, the $P_c M_c$ can be replaced with $P_i M_i$ if it is a larger value. The quantity β is the

weighting factor varying between zero and one that determines whether the scene is composed primarily of trees of a uniform height (and therefore a great deal of mutual shadowing occurs) or of trees of random heights (less mutual shadowing) [27]. The β is given as

$$\beta = \frac{\lambda\Gamma_i}{\lambda\Gamma_i + (h_2 - h_1)/D} \frac{1 - e^{-\lambda\Gamma_i + (h_2 - h_1)/D}}{1 - e^{\lambda\Gamma_i}} \tag{24A}$$

where $\Gamma_i = \pi R^2 \sec\theta_i'$ is the illumination shadow projected on the ground, the quantities h_1 and h_2 are usually ± 2 standard deviations of the mean-height-to center of crown spheroid, and D is the decorrelation depth of a single crown at nadir viewing (defined as $D = R\cot(\frac{\theta_i'}{2})$). The total shadowing cast from single crowns onto other crowns instead of onto the background is given as $M = 1 - \frac{1 - K_g}{\lambda\Gamma}$. P_v is the conditional probability that a crown element will face the sun given that it is mutually shaded from view and P_i is the conditional probability that a crown element will face the viewer given it is mutually shaded from illumination. The terms M_v and M_i are the mutual shadowing proportions of the surface in the view or illumination directions (or indexes of the degree of mutual shadowing occurring in the view or illumination direction). Therefore, each spheroid will usually have a proportion of its ground projected area that will not be viewed (M_v) or not be sunlit (M_i). At the hotspot, M_i and M_v proportions will overlap and there will be no mutual shadowing. The proportion of mutual shadowing in the view direction is given as

$$M_v = 1 - \frac{1 - e^{-\lambda\pi R^2 \sec\theta_v'}}{\lambda\pi R^2 \sec\theta_v'}. \tag{25A}$$

The proportion of mutual shadowing in the illumination direction is given as

$$M_i = 1 - \frac{1 - e^{-\lambda\pi R^2 \sec\theta_i'}}{\lambda\pi R^2 \sec\theta_i'}. \tag{26A}$$

This results in a P_vM_v of

$$P_vM_v = M_v - [1 - \cos(\theta_v' \cos\phi - \theta_i')]/2. \tag{27A}$$

Calculating P_iM_i is not quite as straightforward a computation. Previous work [27] has shown that the boundaries of the mutual shadowing proportion are rather fuzzy and the smaller the amount of mutual shadowing, the fuzzier the boundaries are. Therefore, the P_iM_i is best modeled by

$$P_iM_i = \frac{1 - \cos(\theta_{M_i}[1 - (\theta_i' - \theta_v' \cos\phi)/\pi])}{2} \tag{28A}$$

with $\cos(\theta_{M_i}) = 1 - 2M_i$.

With the terms for f determined, K_c is merely $f(1 - K_g)$ and K_z (the area of shadows) is $1 - K_g - K_c$. Each of these propositions are then multiplied by their component signatures G, C, and Z and summed in (2) to produce the bidirectional reflectance ($R(i, v)$) at a certain view angle under given illumination conditions.

Several complications arise in assuming that these component signatures are Lambertian and can be applied uniformly to the areal proportion [28]. For instance, backgrounds (be they soil or understory) are unlikely to be Lambertian. Shadows will be affected by the multiple scattering of the atmosphere and canopy and should be lighter at the edges. Moreover, the sunlit components can also be altered by multiple scattering and leaf specularity, and therefore are sensitive to the solar illumination angle. If the sunlit component signature used by the model is based on measurements obtained under appropriate illumination conditions, these solar angle dependent effects will be incorporated. Otherwise, an attempt can be made to capture this intensification by modeling the sunlit component signature as a function of solar angle and the amount of crown surface actually exposed to the sun's rays. This results in a sunlit component signature of

$$C = R_c \frac{\mathrm{Proj}(A_c)}{A_c} \tag{29A}$$

where the Lambertian sunlit canopy value R_c is scaled by the ratio of the area of sunlit crown projected onto the background in the illumination direction (in other words the hotspot area $\mathrm{Proj}(A_c)$) to the actual surface area of crown that is sunlit and viewed A_c. This adjusted C is then used in (2A) to produce a bidirectional reflectance.

The bidirectional reflectances ($R(i, v)$) from all the possible view angles can be hemispherically integrated to produce a surface albedo (α) of a scene area under a certain solar illumination. This hemispherical reflectance (direct beam albedo) is given as

$$\alpha = \frac{\int_{2\pi}\int_{\frac{\pi}{2}} R(i, v)\sin\theta_v \cos\theta_v \, d\theta_v \, d\phi_v}{\pi}. \tag{30A}$$

This, then, is the basic Li-Strahler geometric-optical mutual shadowing model for a canopy on flat terrain. Although computationally straightforward, this scheme captures the physical shadowing patterns of a forest canopy. Recent validation studies have shown that the model performs quite well over sparse canopies or canopies with significant variations in crown height [29].

REFERENCES

[1] K. T. Kriebel, "Measured spectral bidirectional reflection properties of four vegetated surfaces," *Appl. Opt.*, vol. 17, pp. 253–258, 1978.

[2] D. S. Kimes and P. J. Sellers, "Inferring hemispherical reflectance of the Earth's surface for global energy budgets from remotely sensed nadir or directional radiance values," *Remote Sensing Environ.*, vol. 18, pp. 205–223, 1985.

[3] D. W. Deering, E. M. Middleton, and T. F. Eck, "Reflectance anisotropy for a spruce-hemlock forest canopy," *Forest Science*, to be published.

[4] W. Verhoef, "Light scattering by leaf layers with application to canopy reflectance modeling: The SAIL model," *Remote Sensing Environ.*, vol. 16, pp. 125–141, 1984.

[5] S. A. W. Gerstl and C. Simmer, "Radiation physics and modeling for off-nadir satellite-sensing of non-Lambertian surfaces," *Remote Sensing Environ.*, vol. 20, pp. 1–29, 1986.

[6] D. S. Kimes, "Radiative transfer in homogeneous and heterogeneous vegetation canopies," in *Photo-Vegetation Interactions*, Myneni and Ross, Eds. Berlin, Germany: Springer-Verlag, 1991, pp. 339–388.

[7] D. S. Kimes, "Modeling the directional reflectance from complete homogeneous vegetation canopies with various leaf-orientation distribution," *J. Opt. Soc. Am.*, vol. 1, pp. 725–737, 1984.

[8] T. Nilson and A. Kuusk, "A reflectance model for the homogeneous plant canopy and its inversion," *Remote Sensing Environ.*, vol. 27, pp. 157–167, 1989.

[9] R. B. Myneni, J. Ross, and G. Asrar, "A review on the theory of photon transport in leaf canopies," *Agric. Forest Meteor.*, vol. 45, 165 pp., 1989.

[10] M. Verstraete, B. Pinty, and R. E. Dickinson, "A physical model of the bidirectional reflectance of vegetation canopies: I Theory," *J. Geophys. Res.*, vol. 95-D8, pp. 11755–11765, 1990.
[11] S. A. W. Gerstl and C. C. Borel, "Principles of the radiosity method versus radiative transfer for canopy reflectance modeling," *IEEE Trans. Geosci. Remote Sensing*, vol. 30, pp. 271–275, 1992.
[12] C. C. Borel, S. A. W. Gerstl, and B. J. Powers, "The radiosity method in optical remote sensing of structured 3-D surfaces," *Remote Sensing Environ.*, vol. 36, pp. 13–44, 1991.
[13] J. Ross and A. Marshak, "Calculation of the canopy bidirectional reflectance using the Monte Carlo methods," *Remote Sensing Environ.*, vol. 24, pp. 213–225, 1988.
[14] J. A. Smith and R. E. Oliver, "Effects of changing canopy directional reflectance on feature selection," *Appl. Opt.*, vol. 13, 1599–1604, 1974.
[15] X. Li and A. H. Strahler, "Geometric-optical modeling of a conifer forest canopy," *IEEE Trans. Geosci. Remote Sensing*, vol. GE-23, pp. 705–721, 1985.
[16] ——, "Geometric-optical bidirectional reflectance modeling of a coniferous forest canopy," *IEEE Trans. Geosci. Remote Sensing*, vol. GE-24, pp. 906–919, 1986.
[17] ——, "Geometric-optical bidirectional reflectance modeling of the discrete-crown vegetation canopy: Effect of crown shape and mutual shadowing," *IEEE Trans. Geosci. Remote Sensing*, vol. 30, pp. 276–292, 1992.
[18] A. H. Strahler and D. L. B. Jupp, "Modeling bidirectional reflectance of forests and woodlands using Boolean models and geometric optics," *Remote Sensing Environ.*, vol. 34, pp. 153–166, 1990.
[19] J. Otterman, "Albedo of a forest modeled as a plane with dense protrusions," *J. Clim. Appl. Meteor.*, vol. 23, pp. 297–307, 1984.
[20] C. E. Woodcock, X. Li, J. Collins, and Y. Wu, "Inversion of the Li-Strahler canopy reflectance model for mapping forest structure I: Calibration and parameter estimation," *IEEE Trans. Geosci. Remote Sensing*, in review.
[21] K. I. Itten and P. Meyer, "Geometric and radiometric correction of TM data of mountainous forested areas," *IEEE Trans. Geosci. Remote Sensing*, vol. 31, pp. 764–770, 1993.
[22] C. Conese, M. A. Gilabert, F. Maselli, and L. Bottai, "Topographic normalization of TM scenes through the use of an atmospheric correction method and digital terrain models," *Photogram. Eng. Remote Sensing*, vol. 59, pp. 1745–1753.
[23] R. Dubayah, "Estimating net solar radiation using Landsat thematic mapper and digital elevation data," *Water Resources Res.*, vol. 9, pp. 2469–2484, 1992.
[24] B. Holben and C. Justice, "The topographic effect on spectral response from nadir-pointing sensors," *Photo. Eng. Remote Sensing*, vol. 46, pp. 1191–1200, 1980.
[25] C. O. Justice, S. W. Wharton, and B. N. Holben, "Application of digital terrain data to quantify and reduce the topographic effect on Landsat data," *Int. J. Remote Sensing*, vol. 2, pp. 213–230, 1981.
[26] K. Hall-Konyves, "The topographic effect on Landsat data in gently undulating terrain in southern Sweden," *Int. J. Remote Sensing*, vol. 8, pp. 157–168, 1987.
[27] X. Li and A. H. Strahler, "Mutual shadowing and directional reflectance of a rough surface: A geometric-optical model," in *Proc., Int. Geosci. Remote Sensing Symp. (IGARSS92)*, Houston, TX, May 1992.
[28] C. Barker Schaaf and A. H. Strahler, "Solar zenith angle effects on forest canopy hemispherical reflectances calculated with a geometric-optical bidirectional reflectance model," *IEEE Trans. Geosci. Remote Sensing*, vol. 31, pp. 921–927, 1993.
[29] ——, "Validation of bidirectional and hemispherical reflectances from a geometric-optical model using ASAS imagery and pyranometer measurements of a spruce forest," *Remote Sensing Environ.*, to be published.

Crystal Barker Schaaf (M'92) received the Ph.D. degree in geography from Boston University in 1994. She received both the S.B. and S.M. degrees in meteorology from the Massachusetts Institute of Technology in 1982, and also received the M.L.A. degree in archaeology from Harvard University in 1988.

She is a research meteorologist in the Satellite Analysis Branch of the Atmospheric Sciences Division, Geophysics Directorate, Phillips Laboratory, Hanscom Air Force Base, MA. Her primary research interests are in the use of remote sensing for automated cloud analyses, the detection of initiating convective clouds, and the characterization of background surfaces, as well as the modeling of reflectances and albedo from anisotropic surfaces.

Xiaowen Li received the B.S. degree from the Chengdu Institute of Radio Engineering, China, in 1968. He received the M.A. degree in geography, the M.S. degree in electrical and computer engineering, and the Ph.D. degree in geography from the University of California at Santa Barbara, in 1981 and 1985.

His permanent position, held since 1987, is Associate Professor in the Institute of Remote Sensing Application of the Chinese Academy of Science, Beijing, China. He is currently Research Professor at the Center for Remote Sensing, Boston University. His primary research interests are in 3-D reflectance modeling and object reconstruction from multiangular remotely sensed images.

Alan H. Strahler (M'86) received the B.A. and Ph.D. degrees in geography from the Johns Hopkins University in 1964 and 1969, respectively.

He is currently Professor of Geography and Researcher in the Center for Remote Sensing, Boston University, Boston, MA. He has held prior academic positions at Hunter College of the City University of New York, at the University of California, Santa Barbara, and the University of Virginia. Originally trained as a biogeographer, he has been actively involved in remote sensing research since 1978. He has been a Principal Investigator on numerous NASA contracts and grants, and is currently a member of the Science Team for the EOS MODIS instrument. His primary research interests are in spatial modeling and spatial statistics as they apply to remote sensing, and in geometric-optical modeling of remotely-sensed scenes. He is particularly interested in remote sensing of forests and the inference of vegetation canopy parameters from digital images through invertible models.

Dr. Strahler was awarded the AAG/RSSG Medal for Outstanding Contributions to Remote Sensing in 1993.